



ELSEVIER

Contents lists available at ScienceDirect

Nuclear Instruments and Methods in Physics Research A

journal homepage: www.elsevier.com/locate/nima

Particle identification in the longitudinally unsegmented RD52 calorimeter

N. Akchurin^a, F. Bedeschi^b, A. Cardini^c, M. Cascella^d, D. De Pedis^f, R. Ferrari^g, S. Fracchia^g, S. Franchino^h, M. Fraternali^e, G. Gaudio^g, P. Genova^e, J. Hauptmanⁱ, L. La Rotonda^j, S. Lee^a, M. Livan^e, E. Meoni^k, D. Pinci^f, A. Policicchio^j, J.G. Saraiva^l, F. Scuri^b, A. Sill^a, T. Venturelli^j, R. Wigmans^{a,*}

^a Texas Tech University, Lubbock, TX, USA^b INFN Sezione di Pisa, Italy^c INFN Sezione di Cagliari, Monserrato, CA, Italy^d Dipartimento di Fisica, Università di Salento, and INFN Sezione di Lecce, Italy^e INFN Sezione di Roma, Italy^f INFN Sezione di Pavia, Italy^g CERN, Genève, Switzerland^h INFN Sezione di Pavia and Dipartimento di Fisica, Università di Pavia, Italyⁱ Iowa State University, Ames, IA, USA^j Dipartimento di Fisica, Università della Calabria, and INFN Cosenza, Italy^k Tufts University, Medford, MA, USA^l LIP, Lisbon, Portugal

ARTICLE INFO

Article history:

Received 30 June 2013

Received in revised form

30 August 2013

Accepted 3 September 2013

Available online 18 September 2013

Keywords:

Dual-readout calorimetry

Cherenkov light

Particle identification

ABSTRACT

The RD52 dual-readout calorimeter is a longitudinally unsegmented instrument intended for the detection of both electromagnetically and hadronically interacting particles with unprecedented precision. In this paper, the identification of the showering particles and, in particular, the identification of electrons and γ s with this instrument are investigated. The techniques used for this purpose include differences in the shower development observed with scintillation light and Cherenkov radiation, the radial shower profile of the particles and the time structure (including the starting point) of the calorimeter signals. It turns out that, at 60 GeV, electrons can be correctly identified in 99.8% of the cases, by means of criteria that eliminate 99.8% of the hadrons.

© 2013 Elsevier B.V. All rights reserved.

1. Introduction

Traditionally, the calorimeter systems in high-energy physics experiments have been separated into two sections: the electromagnetic (em) and the hadronic section. This arrangement offers a certain number of advantages, especially for the identification of electrons and photons, which deposit all their energy in the em section and can thus be identified as such based on this characteristic. Also, since the em section represents typically only a few percent of the total mass, more expensive materials (e.g., crystals) can be used in order to optimize its performance.

Yet, there are also substantial disadvantages, especially for what concerns the detection of hadron jets. Hadrons deposit typically some fraction of their energy in each section, with very

large event-to-event fluctuations in the energy sharing between the two sections. The response, i.e., the average signal per GeV deposited energy, is typically considerably smaller for hadrons than for electrons of the same energy. This is a consequence of the fact that in hadron showers a considerable fraction of the energy is used to break up atomic nuclei, and this energy does not contribute to the calorimeter signals. This energy fraction is, on average, dependent on the energy of the showering particles, and varies strongly from event to event. These characteristics lead to problems in determining the energy of the showering hadrons and jets, since it is not obvious how to convert the measured signals into deposited energy.

The RD52 Collaboration has demonstrated that these so-called *jet energy scale* problems can be avoided in so-called dual-readout calorimeters [1–3]. In these devices, the precision with which the energy of single hadrons and jets can be measured is greatly improved by simultaneous measurements of the deposited energy and the fraction of that energy carried by relativistic charged

* Corresponding author. Tel.: +1 806 742 3779; fax: +1 806 742 1182.

E-mail addresses: Richard.Wigmans@ttu.edu, wigmans@ttu.edu (R. Wigmans).

shower particles, which are predominantly electrons and positrons. These measurements make it possible to measure the em component of these showers (f_{em}) event by event. In this way, the effects of fluctuations in f_{em} , which tend to dominate the hadronic energy resolution of calorimeters, are eliminated, and the response can be trivially equalized to that of purely em showers (for which $f_{em}=1$), such as the ones generated by electrons.

In the RD52 calorimeter, the two types of signals are generated in scintillating fibers, which measure the deposited energy, and in clear plastic fibers, which measure the relativistic shower particles, by means of the Cherenkov light generated by these. A large number of such fibers are embedded in a metal absorber structure. This detector is longitudinally unsegmented. It is calibrated with electrons, and the calibration constants established in this way also provide the correct energy for hadronic showers developing in it. Recently, a 1.5-ton detector of this type was exposed to particle beams at the CERN Super Proton Synchrotron. In this paper, we investigate to what extent it is possible to distinguish between different types of particles, and especially between electrons and hadrons, with the signals provided by this detector. Identification of isolated electrons, pions and muons would be of particular importance for the study of the decay of Higgs bosons into pairs of τ leptons, if a calorimeter of this type were to be used in an experiment at a future Higgs factory.

In Section 2, the instruments and the experimental setup in which the measurements were carried out are described, as well as the calibration and data analysis methods that were used. Experimental results are presented in Section 3. In the concluding Section 4, we discuss these results and their implications.

2. Equipment and measurements

2.1. Detectors and beam line

The measurements described in this paper were performed in the H8 beam line of the Super Proton Synchrotron at CERN. Beams of high-energy particles were steered into the RD52 fiber calorimeter. A system of auxiliary detectors, described below, was used to select the beam particles that entered the calorimeter in a well defined, small area. The experimental setup is shown in Fig. 1.

The fiber calorimeter is modular. Each module is 2.5 m long ($10\lambda_{int}$), and has a cross-section of 9.2×9.2 cm². Each module consists of four towers ($4.6 \times 4.6 \times 250$ cm³), and each tower contains 1024 plastic optical fibers (diameter 1.0 mm, equal numbers of scintillating and clear plastic fibers).¹ Each tower produces two signals, a scintillation signal and a Cherenkov signal, which are detected by separate PMTs.² For this reason, this type of detector is also known as a DREAM (Dual-REAdout Method) calorimeter.

The first modules were constructed with lead as absorber material. In the course of 2012, we also managed to construct modules with copper as absorber material (Fig. 2). The fiducial mass of the latter was ~ 120 kg, instead of 150 kg for a lead based module. One of these modules was equipped with Cherenkov fibers of which the upstream end was aluminized.³ Fig. 2 shows the basic structure of the modules for which lead (a) or copper (b) was used as absorber material. The sampling fraction for minimum ionizing particles, both for the scintillation and for the Cherenkov sampling structure, is 5.3% for the lead-based calorimeter and 4.6% for the copper-based one.

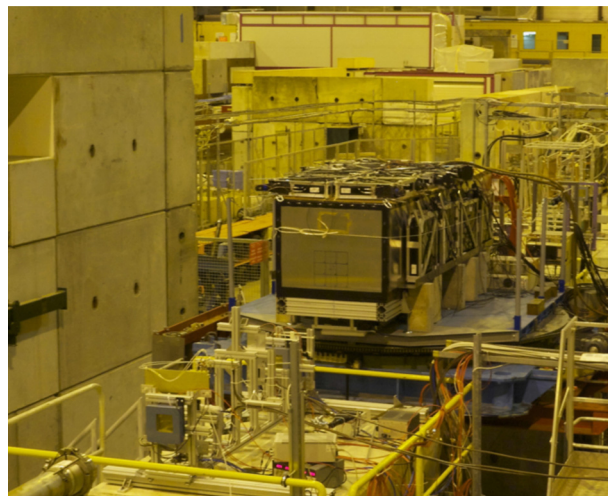


Fig. 1. The new SuperDREAM fiber calorimeter, installed in the H8C beam area. The system of trigger counters and beam defining elements is visible in the left bottom part of the figure.

By the end of 2012, nine lead-based modules and two copper-based ones were ready to be tested at CERN, just before the start of the two-year shutdown of the accelerator complex. These modules were assembled together, as shown in Fig. 3, and tested as such in November/December 2012.

Measurements of the radial shower profile showed that the showers initiated by 60 GeV π^- entering the detector within a few cm of its geometric center were, on average, contained at the level of 93.6%. In order to detect the shower leakage, the calorimeter was surrounded by large slabs of plastic scintillator ($50 \times 50 \times 10$ cm³, mass 25 kg). Twenty such counters were used in these tests. They can be seen in Fig. 1 on the top, the bottom and the right hand side of the box containing the calorimeter. Since em showers were contained to better than 99% in this calorimeter, shower leakage was not an issue for electrons and photons.

The experimental setup contained also a number of auxiliary detectors, which were intended to determine the identity of individual beam particles, and to measure their trajectory. Fig. 4 shows a schematic overview of the beam line, in which the positions of these auxiliary counters are indicated:

- Two small scintillation counters provided the signals that were used to trigger the data acquisition system. These Trigger Counters (T1, T2) were 2.5 mm thick, and the area of overlap was 4×4 cm². A coincidence between the logic signals from these counters provided the trigger.
- The trajectories of individual beam particles could be reconstructed with the information provided by two small drift chambers (DC1, DC2), which were installed upstream and downstream of the trigger counters. This system made it possible to determine the location of the impact point of the beam particles at the calorimeter with a precision of about 1 mm.
- About 80 cm upstream of the calorimeter, a preshower detector (PSD) provided the signals needed to remove pions and muons contaminating the electron beams. This PSD consisted of a 5 mm thick lead plate, followed by a 5 mm thick plastic scintillator. Electrons started developing showers in this device, while muons and hadrons typically produced a signal characteristic for a minimum ionizing particle (mip) in the scintillator plate.
- Downstream of the calorimeter (DREAM), a tail catcher (TC) served to identify pions and muons that were not completely absorbed in the $10\lambda_{int}$ deep calorimeter structure. This tail catcher consisted of a simple 20×20 cm² scintillation counter.

¹ The scintillating fibers were of the type SCSF-78, produced by Kuraray, the Cherenkov light was generated in PMMA based SK40 fibers, produced by Mitsubishi.

² Hamamatsu R8900, 10-stage.

³ This was done at Fermilab, by Eileen Hahn and Erik Ramberg.

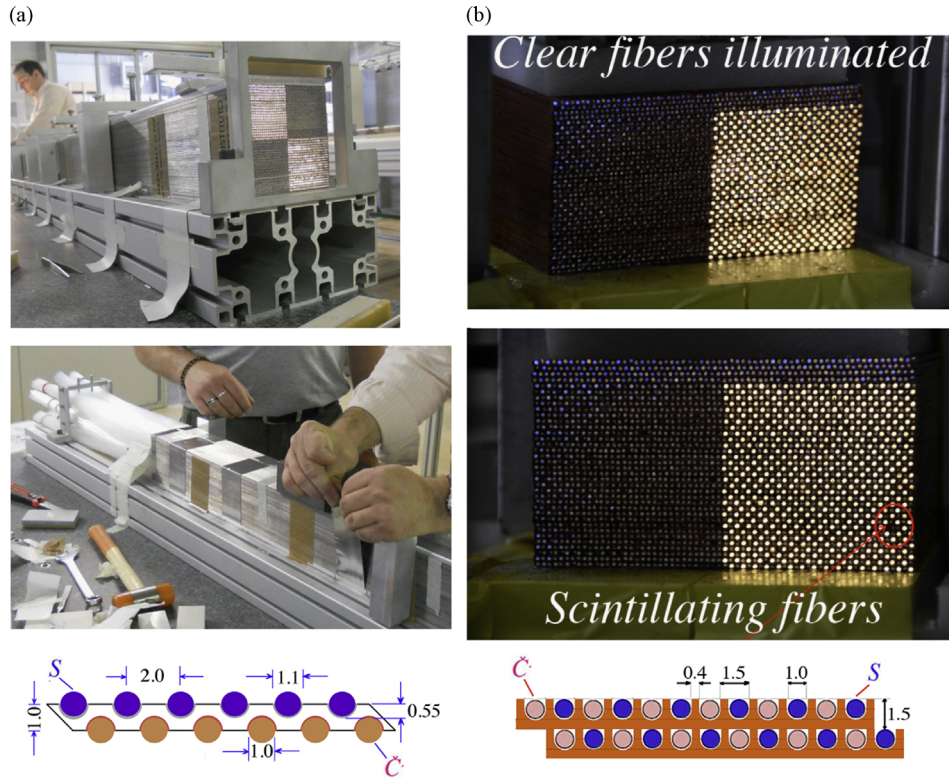


Fig. 2. Pictures of the first RD52 modules built with lead (left, a) or copper (right, b) as absorber material, as well as the basic structure of these new calorimeters. The dimensions are given in millimeters.

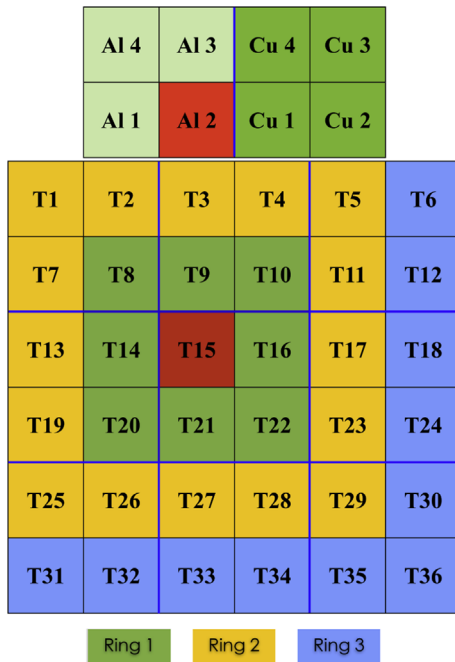


Fig. 3. The RD52 calorimeter as tested at the end of 2012. It consisted of 9 lead-based modules, each consisting of 4 towers (towers 1–36), and two copper-based modules, placed on top of the lead array. The left copper module (of which the towers are marked as “Al”) is equipped with Cherenkov fibers with an aluminized upstream end face. For the measurements described in this paper, the particle beams were typically steered in the center of tower T15.

- Further downstream of the calorimeter, behind an additional $8\lambda_{\text{int}}$ worth of absorber, a $50 \times 50 \text{ cm}^2$ scintillation counter (μ) served to identify muons that contaminated the particle beam.

The system of drift chambers, trigger counters and PSD can be seen in the bottom left corner of Fig. 1.

2.2. Data acquisition

In order to minimize delays in the DAQ system, we used special 15-mm diameter low-loss cables to transport the signals from the trigger counters to the counting room. The signal speed in these cables was measured to be 0.78c. The calorimeter signals, as well as the signals from the auxiliary counters that needed to be digitized (PSD, tail catcher, muon counter) were transported through RG-58 cables with (for timing purposes) appropriate lengths to the counting room.

There, the signals to be digitized were fed into charge ADCs. The signals from the wire chambers were fed into TDCs. The time information could be converted into (x, y) coordinates of the point where the beam particle traversed the chamber. The two signals from Tower 15 (see Fig. 3) were also fed into TDC channels. These TDC channels were started by the signal produced by trigger counter T1 upon the passage of a charged beam particle, and stopped when the tower 15 signals crossed a preset discriminator level.

The data acquisition system used VME electronics. Two VME crates hosted all the needed readout and control boards. The signals from the calorimeter channels and the auxiliary detectors were integrated and digitized with a sensitivity of 100 fC/count, on 12-bit QDC V792 CAEN modules. The timing information of the tracking chambers was recorded with 1 ns resolution in a 16-bit 16-channel CAEN V775N TDC, while the starting time of the Tower 15 signals was measured with 0.14 ns resolution.

Our readout scheme optimized the CPU utilization and the data taking efficiency thanks to the bunch structure of the SPS cycle, where beam particles were provided to our experiment during a spill of 9.6 s, with a repetition period of 48 s.

2.3. Experimental data and analysis methods

The measurements described in this paper were performed in the H8 beam of the CERN Super Proton Synchrotron. We used secondary beams with energies of 20, 60 and 80 GeV for our purpose. These secondary beams consisted predominantly of pions and muons. Beams enriched in electrons were derived from the secondary 80 GeV beam, by sending the beam particles through a 5 mm thick lead radiator. In practice, only the electron component of the secondary beam lost a substantial energy fraction passing through this material, and electrons of the desired momentum

(20 or 60 GeV) were selected with properly tuned downstream bending magnets.

The measurements were performed by steering the beams into the center of Tower 15. Typically, for each run 50 000 events were collected. In each run, 10% randomly triggered events provided pedestal information. For each event, the ADC information of all calorimeter towers was recorded, as well as the ADC data from the auxiliary detectors (muon counter, PSD, tail catcher), and the TDC data from both Tower 15 signals and the wire chambers.

Off-line, the beam chamber information could be used to select events that entered the calorimeter in a small (typically

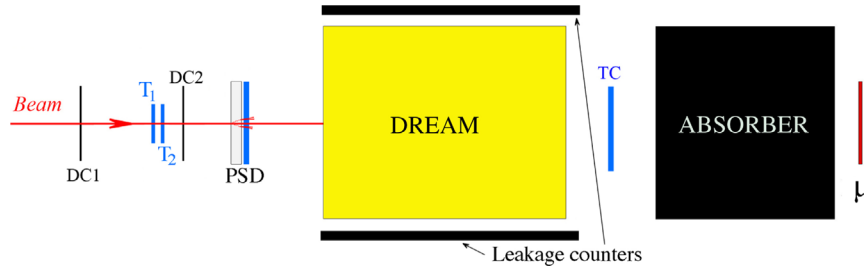


Fig. 4. Schematic overview of the arrangement of the auxiliary detectors that were used to identify the individual beam particles (not to scale). See text for details.

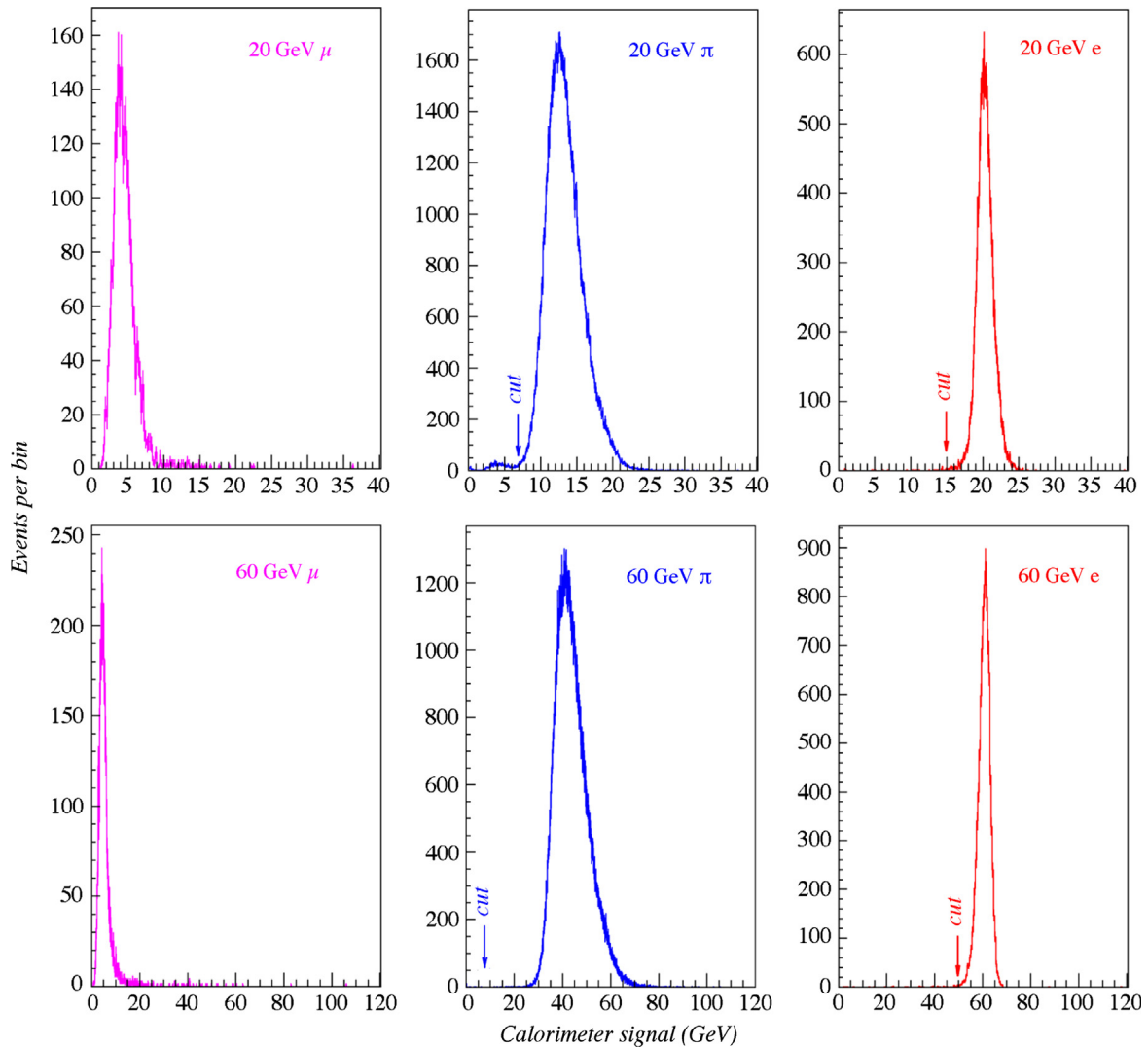


Fig. 5. The calorimeter signal distributions for the pure muon, pion and electron event samples used in the analyses. See text for details.

$10 \times 10 \text{ mm}^2$) region located near its geometric center. This was done both at 20 GeV and at 60 GeV. The information provided by the auxiliary detectors was used to identify each event either as an electron, a muon or a pion.

The analyses described in Section 3 were performed on pure event samples of electrons, muons and pions, with the goal to determine to what extent the calorimeter information *alone* could be used to identify these beam particles, and to measure the identification and mis-identification probabilities for each particle type and energy. To that end, the following cuts were applied:

- (1) *Electrons* were identified as particles that produced a signal in the PSD that was larger than ~ 200 ADC counts above pedestal, which corresponds to the combined signals produced by 2 minimum ionizing particles (mips) traversing this detector. Additional requirements were that no signals incompatible with electronic noise were produced in the tail catcher and the muon counter. The total scintillation signal in the calorimeter should be larger than 15 GeV for the 20 GeV beam and larger than 50 GeV for the 60 GeV beam.
- (2) *Pions* were identified as particles that produced a signal in the PSD that was compatible with a minimum ionizing particle traversing it ($0.5 < \text{signal} < 2.0$ mip), and no signal incompatible with noise in the muon counter. The total scintillation signal in the calorimeter should be larger than 7 GeV.
- (3) *Muons* were identified as particles that produced signals in the PSD, the tail catcher and the muon counter that were compatible with minimum ionizing particles traversing these detectors.

Fig. 5 shows the results of the cleanup procedures for the 20 and 60 GeV beam. Shown are the total scintillation signal distributions for events that were classified as muons, pions and electrons based on the information from the preshower detector, the tail catcher and the muon counter. The pion samples contained a small contamination of muons that did not produce a signal in the muon counter, because of multiple scattering or inefficiencies of this counter. This contamination was removed by the cuts indicated in the figure.

2.4. Calibration

The calibration of the calorimeter towers was performed with 20 GeV electrons. A beam of these electrons, selected to form a $20 \times 20 \text{ mm}^2$ beamspot by means of the beam chambers, was steered into the centers of each of the $36+8$ calorimeter towers. In an analysis described elsewhere [4], we found that the electrons deposited, on average, 85% of their energy in the hit tower, the rest was distributed over all other towers. We also found that the energy sharing between the different towers contributing to the total signals was not significantly different for the scintillation and Cherenkov signals. The average signals observed in the hit towers during the calibration runs thus corresponded to 17 GeV, for both types of signals, and the calibration constants were calculated accordingly, in terms of GeV per ADC count.

The electrons deposited typically 0.5–1% of their energy in the preshower detector. The effects of that on the calorimeter signals were insignificant for the present analyses.

3. Experimental results

3.1. Shower profiles

In traditional calorimeters, composed of an em and an hadronic section, electron/pion separation is achieved because of the fact that in high- Z absorbers the longitudinal size of hadron showers is typically much larger than that of em showers of the same energy.

Therefore, the energy fraction deposited in the em calorimeter section is much larger for electrons and photons than for hadrons. However, similar differences apply to the *lateral* shower size, which can therefore also be used to distinguish between em and hadron showers.

One advantage of the RD52 calorimeter structure is that the lateral granularity can be made arbitrarily small, one can make the tower size (defined by the number of fibers connected to one readout element) as large or small as desired. The lateral size of the RD52 calorimeter towers is 1.6×1.6 Moliere radii, or 0.2×0.2 nuclear interaction lengths, which is considerably smaller than the granularity of typical calorimeter systems used in modern high-energy physics experiments. Our measurements show that electrons hitting a tower in its central region deposit typically 85% of their energy in that tower. For hadrons, the corresponding number is much smaller, typically 40–50%.

Fig. 6 shows the distribution of the fraction of the shower energy deposited in the hit tower (f_{hit}) by electrons and by π^- beam particles, at 20 GeV (Fig. 6a) and 60 GeV (Fig. 6b). At the higher energy, the distribution for electrons is narrower, but concentrated around the same average value. This confirms that the average lateral em shower profile is practically energy independent. Just like for the response function, the larger width at 20 GeV is the result of increased event-to-event fluctuations. The figure also shows that the average energy deposited by pions in the hit tower clearly increases with the energy of the beam particles. This is a consequence of the fact that the average em shower fraction increases with the hadron energy, the same phenomenon that is responsible for the signal non-linearity in (non-compensating) hadron calorimeters [5].

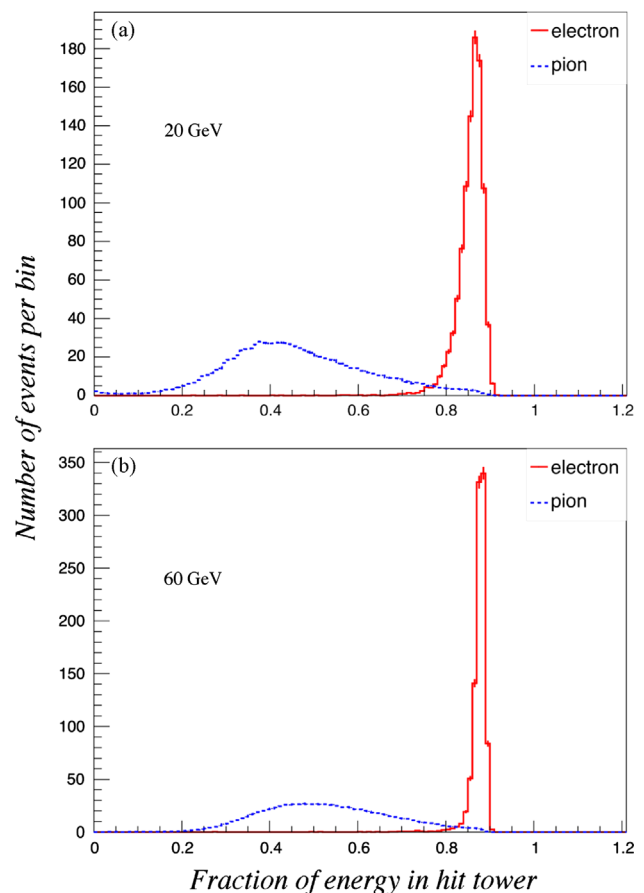


Fig. 6. Distribution of the energy fraction deposited in the hit tower by electrons and pions showering in the RD52 calorimeter. Data for 20 GeV (a) and 60 GeV (b) beam particles.

As a result of these two phenomena, the effective separability of electrons and pions on the basis of the lateral shower profile does not change much as a function of energy, since the effects tend to cancel each other. Good separation is achieved for f_{cut} values between 0.7 and 0.8. Table 1 summarizes the efficiency for electron recognition, as well as the probability for mis-identifying a pion as an electron, for a number of f_{cut} values in this range.

It should be emphasized that these results, strictly speaking, only apply to particles entering the calorimeter in a small region around the center of a tower. However, because of the extremely collimated nature of em showers, the results are not very different for other impact points. For example, we measured that electrons

entering a tower as close as 5 mm from the boundary with a neighboring tower still deposit more than 75% of their total energy in that tower. In such cases, where a significant fraction of the energy is deposited in another tower than the one in which the particle entered the calorimeter, one might use the fraction of the total energy deposited in the sum of the two towers with the largest signals as the figure of merit. We found that the e/π separability in such cases is similar to the one listed in Table 1.

Table 1

The electron identification efficiency and the probability for mis-identifying a pion as an electron, for various choices of the parameter f_{cut} . A particle is defined as an electron/pion when the fraction of the total shower energy detected in the hit calorimeter tower (f_{hit}) is larger/smaller than the value of f_{cut} . The statistical uncertainties are in all cases smaller than 0.1%.

f_{cut}	20 GeV		60 GeV	
	e id (%)	π mis-id (%)	e id (%)	π mis-id (%)
0.70	99.3	8.4	99.6	13.2
0.72	99.1	6.9	99.5	10.7
0.74	98.8	5.6	99.3	8.5
0.76	98.1	4.5	99.2	6.7
0.78	97.1	3.5	99.1	5.1
0.80	94.6	2.7	98.8	3.8
0.82	92.3	2.4	98.5	3.2

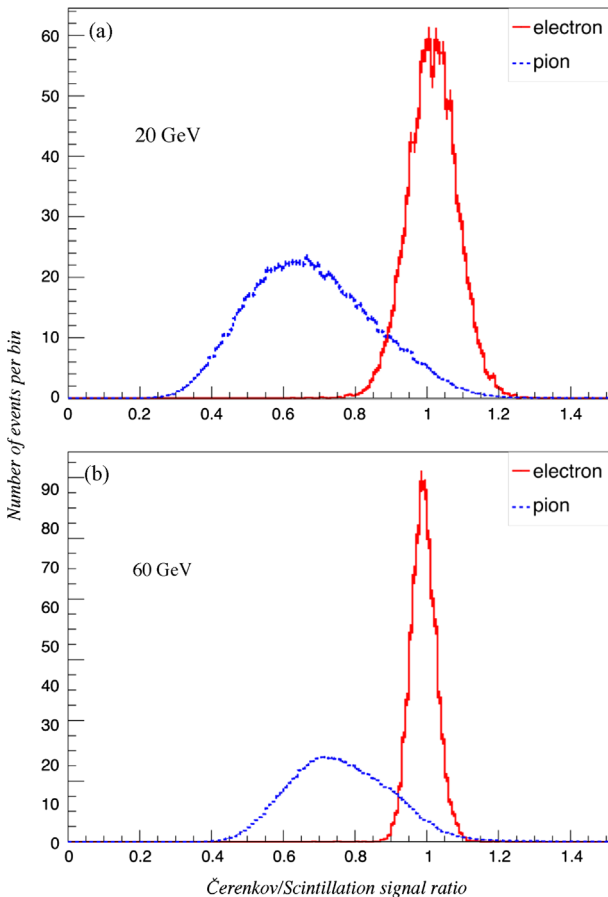


Fig. 7. Distribution of the C/S signal ratio in the hit tower for electrons and pions showering in the RD52 calorimeter. Data for 20 GeV (a) and 60 GeV (b) beam particles.

3.2. Cherenkov/scintillator comparison

A unique aspect of the RD52 calorimeter is the fact that two types of signals are produced: scintillation (S) signals and Cherenkov (C) signals. This offers possibilities for particle identification which are not available in other types of calorimeters. One variable which is quite effective in distinguishing electrons from pions is the ratio of the two types of signals, C/S . Since the tower signals are calibrated with electrons, this ratio is typically around 1.0 for electron showers, while it is smaller than 1.0 for hadron showers.

Fig. 7 shows the distribution of the C/S signal ratio for electrons and π^- beam particles, at energies of 20 (Fig. 7a) and 60 GeV (Fig. 7b). Just like in the case of the lateral shower profile (Fig. 6), the electron distribution becomes narrower as the energy increases, while the distribution for the pions shifts to larger values, from an average of ~ 0.6 to ~ 0.7 , and the reasons are the same as the ones given for the lateral shower profile. The width of the electron distribution shrinks because of the reduced effects of event-to-event fluctuations, while the average value of the C/S signal ratio for pion showers increases because of the increased em shower fraction. And also here, these effects affect the electron/pion separability in opposite ways and tend to cancel each other in that respect.

The best separation is achieved for $(C/S)_{\text{cut}}$ values around 0.9. Table 2 summarizes the efficiency for electron recognition, as well as the probability for mis-identifying a pion as an electron, for a number of $(C/S)_{\text{cut}}$ values.

3.3. Time structure

3.3.1. The start time of the PMT signals

Measurements of the average depth at which the light is produced inside the calorimeter provide a powerful tool to distinguish between showers initiated by electrons or hadrons. In earlier studies of longitudinally unsegmented calorimeters, this depth was measured from the displacement of the lateral center-of-gravity with respect to the entrance point of the beam particles. To use this method, it was necessary to rotate the calorimeter over a small angle with respect to the beam line [1]. In the present study, we have explored a different method to measure this depth, which does not require such a rotation.

Table 2

The electron identification efficiency and the probability for mis-identifying a pion as an electron, for various choices of the parameter $(C/S)_{\text{cut}}$, which defines a particle as an electron/pion when its C/S value is larger/smaller than $(C/S)_{\text{cut}}$. The statistical uncertainties are in all cases smaller than 0.1%.

$(C/S)_{\text{cut}}$	20 GeV		60 GeV	
	e id (%)	π mis-id (%)	e id (%)	π mis-id (%)
0.80	99.8	24.0	99.97	38.0
0.82	99.7	22.5	99.96	35.6
0.84	99.5	19.5	99.95	31.0
0.86	99.0	16.9	99.95	26.7
0.88	98.1	14.5	99.93	22.6
0.90	96.4	12.4	99.8	18.9
0.92	91.8	9.5	98.0	13.9

And unlike the displacement method, it is also expected to work for jets and neutral particles.

This new method is based on the fact that the light in the optical fibers travels at a lower speed than the particles that generate this light. The effective speed of the light generated in the fibers is c/n , with n the index of refraction. For an index of 1.59, typical for polystyrene based fibers, this translates into a speed of 17 cm/ns. On the other hand, the shower particles that are responsible for the generation of

light in the fibers typically travel at a speed close to c . The effects of this are illustrated in Fig. 8, which shows how the starting time of the PMT signal varies with the (average) depth at which the light is produced inside the calorimeter.

The deeper inside the calorimeter the light is produced, the earlier the PMT signal. For the polystyrene fibers, the effect amounts to 2.55 ns/m. For the tested calorimeter, which had an effective nuclear interaction length (λ_{int}) of ~ 27 cm, this corresponds to ~ 0.6 ns/ λ_{int} .

We tested this method experimentally with 60 GeV electron and pion event samples, using the TDC readout of Tower 15. The TDC was started by the signal produced by trigger counter T1, and stopped by the signal from Tower 15. Fig. 9a shows the TDC signal distribution for the electron showers. In these showers, the light is, on average, produced at a depth of ~ 12 cm inside the calorimeter ($10X_0$), with event-to-event variations at the level of a few cm. The width of this distribution, ~ 0.5 ns, is thus a good measure for the

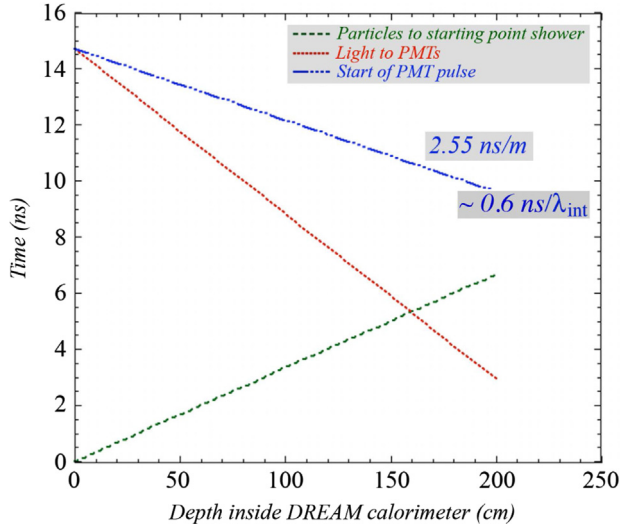


Fig. 8. Dependence of the starting time of the PMT signals on the average depth (z) inside the calorimeter where the light is produced (the dash-dotted line). This time is measured with respect to the moment the particles entered the calorimeter. Also shown are the time it takes the particles to travel to z (the dashed line) and the time it takes the light to travel from z to the PMT (the dotted line).

Table 3

The electron identification efficiency and the probability for mis-identifying a pion as an electron, for various choices of the parameter $t_s(\text{cut})$, which defines a particle as an electron/pion when the starting time of its PMT signal is larger/smaller than $t_s(\text{cut})$. Data for the scintillation signals from 60 GeV beam particles. The statistical uncertainties are in all cases smaller than 0.1%.

$t_s(\text{cut})$ (ns)	e id (%)	π mis-id (%)
28.0	99.5	15.0
28.2	99.1	11.3
28.4	97.5	5.9
28.6	95.8	4.1
28.8	88.7	1.9
29.0	82.5	1.2
29.2	74.0	0.8

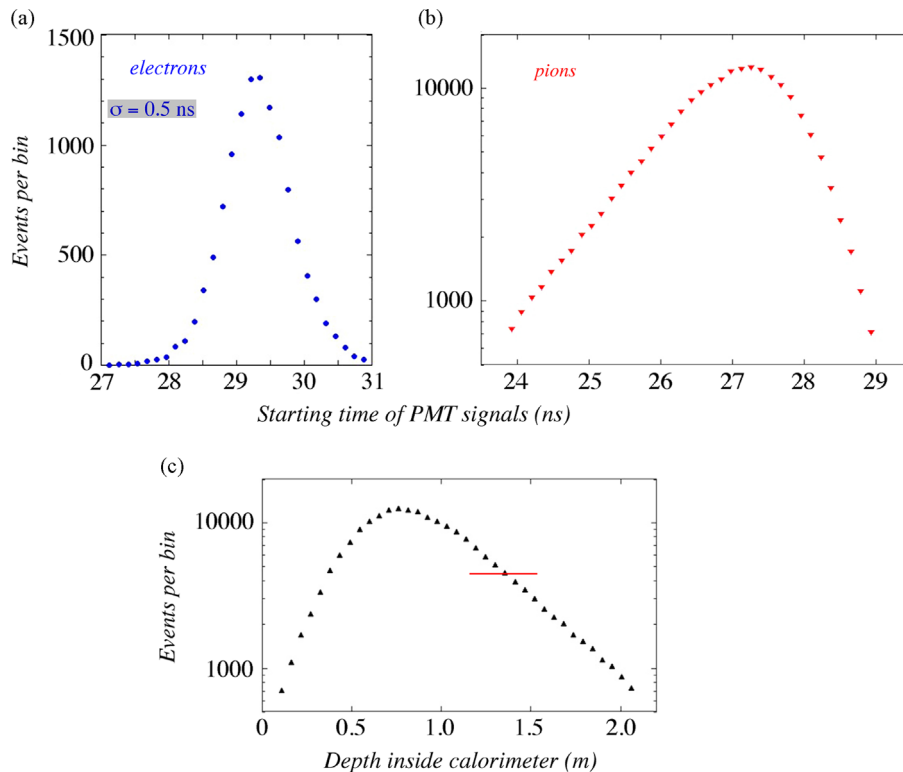


Fig. 9. The measured distribution of the starting time of the calorimeter's scintillation signals produced by 60 GeV electrons (a) and 60 GeV pions (b). This time is measured with respect to the moment the beam particle traversed trigger counter T1, installed upstream of the calorimeter (see Fig. 4). These data were used to determine the distribution of the average depth at which the light was produced in the hadron showers (c).

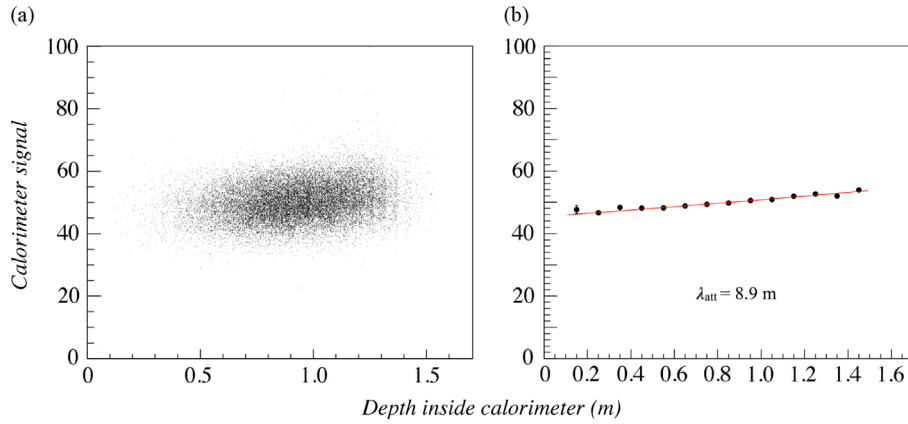


Fig. 10. Light attenuation in the Cherenkov fibers. The scatter plot (a) shows the calorimeter signal for the Cherenkov light from 80 GeV π^- versus the average depth at which that light was produced inside the calorimeter. The projection of this scatter plot on the vertical axis provides the effective light attenuation curve of the fibers (b).

precision with which the depth of the light production can be determined for individual events, ~ 20 cm.

Fig. 9b shows the measured TDC distribution for 60 GeV π^- . This distribution peaks ~ 1.5 ns earlier than that of the electrons, which means that the light is, on average, produced 60 cm deeper inside the calorimeter. The distribution is also asymmetric, it has an exponential tail towards early starting times, i.e., light production deep inside the calorimeter. We used this measured TDC signal distribution to reconstruct the typical depth at which the light was produced for individual pion showers. The result, shown in Fig. 9c, resembles the longitudinal shower profile of the 60 GeV pion showers in this calorimeter.

These data illustrate that the starting point of the PMT signals may well be used to distinguish between electron and pion events. We have investigated how well this works for our individual event samples, using a TDC signal corresponding to a starting time of $t_s(\text{cut})$ after the trigger signal as the discriminating variable. Events with $t_s > t_s(\text{cut})$ were classified as electrons, events with $t_s < t_s(\text{cut})$ as pions. Table 3 summarizes the efficiency for electron recognition, as well as the probability for mis-identifying a pion as an electron, for a number of $t_s(\text{cut})$ values.

Strictly speaking, these results are slightly biased, since the electrons were selected on the basis of the fact that they produced a shower signal in the PSD, whereas the pions were required to traverse that detector without starting a shower. In the absence of this $1X_0$ thick PSD, the electron starting point (Fig. 9a) would, on average, shift by 0.02 ns. This would slightly increase the pion misidentification efficiencies. The effects of this were determined to be smaller than 5% in all cases.

Apart from particle identification, the measurement of the depth of the light production in this longitudinally unsegmented calorimeter may also turn out to be useful for other purposes. For example, it may be used to correct for the effects of light attenuation in the fibers on the calorimeter signals. Fig. 10 shows results of measurements performed in this context. The scatter plot in Fig. 10a shows the calorimeter signal for the Cherenkov light from 80 GeV π^- versus the average depth at which that light was produced inside the calorimeter. As the light is produced deeper inside, the signal tends to be, on average, somewhat larger. This effect is quantified in Fig. 10b, which shows the average signal as a function of the depth at which the light was produced. The data points are well described with an exponential curve with a slope of 8.9 m, which thus represents the attenuation length of these fibers. This may seem long, but one should realize that hadron showers fluctuate longitudinally on a scale of one λ_{int} . Over that length, the signal changes by 2–3% as a result of light

attenuation. And since this calorimeter is intended for hadronic energy measurements at the level of 1–2%, elimination of the energy independent term caused by light attenuation effects is important.

Apart from the mentioned applications, the depth measurement in several neighboring towers contributing to the shower signal may provide an indication of the *direction* at which the particle(s) entered the calorimeter, thus allowing measurement of the entire four-vector. This will be the topic of a future study.

3.3.2. The pulse width

About 20 years ago, another aspect of the time structure of the calorimeter signals was used to distinguish between electron and pion showers in a longitudinally unsegmented calorimeter. The SPACAL collaboration used the pulse width at 20% of the amplitude (FWFM) to this end [6] and measured very significant differences between the distributions of this variable for electrons and pions. In their case, the differences were considerably increased by the fact that the upstream ends of their fibers were made reflective. Therefore, the deeper inside the calorimeter the (scintillation) light was produced, the wider the pulse.

We also tried to use the width of the calorimeter signals to distinguish electron from pion showers. Unlike SPACAL, we could not benefit from the mentioned broadening effect, since the upstream ends of the RD52 (Pb based) calorimeter were not reflective. However, the fact that the light production is spread out over a certain area in depth also led to a larger signal width, since the arrival time of the light at the PMT surface depends on the depth at which it was produced. We analyzed data from earlier beam tests of individual calorimeter modules (Pb based) for this purpose, as described in Section 2.1 and shown in Fig. 2. The signals from the 4 towers of this module were grouped together, and the time structure of the calorimeter signals formed this way was recorded by means of a Tektronix TDS 7254B digital oscilloscope,⁴ which provided a sampling capability of 5 GSample/s, at an analog bandwidth of 2.5 GHz, over 4 input channels. For these tests, only 2 channels were sampled. The oscilloscope gain (scale) was tuned such as to optimize the exploitation of the 8-bit dynamic range, i.e., by choosing the sensitivity such that the overflow rate was $\lesssim 1\%$.

For pion showers, mainly the electromagnetic core was contained in one such module, and therefore the pion signals differed much less from the electron ones than if the entire shower would

⁴ http://www.tek.com/site/ps/0,,55-13766-SPECS_EN,00.html

have been detected. Yet, clear evidence for the broadening of the pion signals was observed in these measurements, which were performed for electrons and pions at 30 and 80 GeV. Fig. 11 shows the distribution of the ratio of the integrated charge and the amplitude of the signals. This ratio is typically larger for the pion signals compared to the electron ones, and reflects the increased width of the pion signals. The figure, and Table 4, where details of the electron/pion separation as a function of the parameter $(Q/A)_{\text{cut}}$ are listed, show that the electron/pion separation that can be achieved on the basis of this event characteristic is comparable for the two energies, but not spectacular.

However, since the effects responsible for the electron/pion difference are very different from the ones that determine the difference in the starting time of the PMT signals, the combined

information may be considerably better than that for either of the timing-based methods.

3.4. Combining the different e/π separation methods

One may wonder to what extent the different methods described in the previous subsections are correlated, in other words to what extent the mis-identified particles are either the same or different ones for each method. We investigated this issue for the 60 GeV particles, for which data obtained with three different methods were available. The cuts were chosen such as to achieve a preset overall electron efficiency, e.g., 99%, 98%, etc. and to select the pions that passed all the cuts used to achieve this. We also used multivariate data analysis for this purpose [9].

It turns out that by combining different e/π separation methods, important improvements can be achieved in the capability of our longitudinally unsegmented calorimeter to identify electrons with minimal contamination of mis-identified particles. For example, 99.1% of electrons and less than 0.5% of the pions passed the combination of the cuts $f_{\text{cut}} > 0.70$ and $t_s(\text{cut}) > 28.0$ ns. This illustrates that these two types of cuts are completely uncorrelated, which is no surprise since the first cut discriminates on the basis of the lateral shower shape, and the second cut on the depth at which the pion shower started. Using the Cherenkov/scintillation characteristics, a cut $(C/S)_{\text{cut}} > 0.85$ further improved the purity of the electron sample. The remaining mis-identified pions are predominantly particles that interact close to the front face of the calorimeter and transfer a large fraction of their energy to one or several π^0 s. Charge exchange reactions ($\pi^- + p \rightarrow \pi^0 + n$) fall into this category.

Of course, there are in principle many different combinations of cuts that achieve approximately the same results as quoted above. The multivariate neural network analysis showed that the best e/π separation achievable with the three variables used for the 60 GeV beams was 99.8% electron identification with 0.2% pion misidentification (for $MLP > 0.17$, see Fig. 12). Further improvements may be expected by including the full time structure information of the pulses, especially if the upstream ends of the fibers are made reflective [6].

Finally, we want to point out that any electron contamination of the pion sample, for example by electrons that traversed the PSD producing a signal equivalent to that of a mip, would set an upper

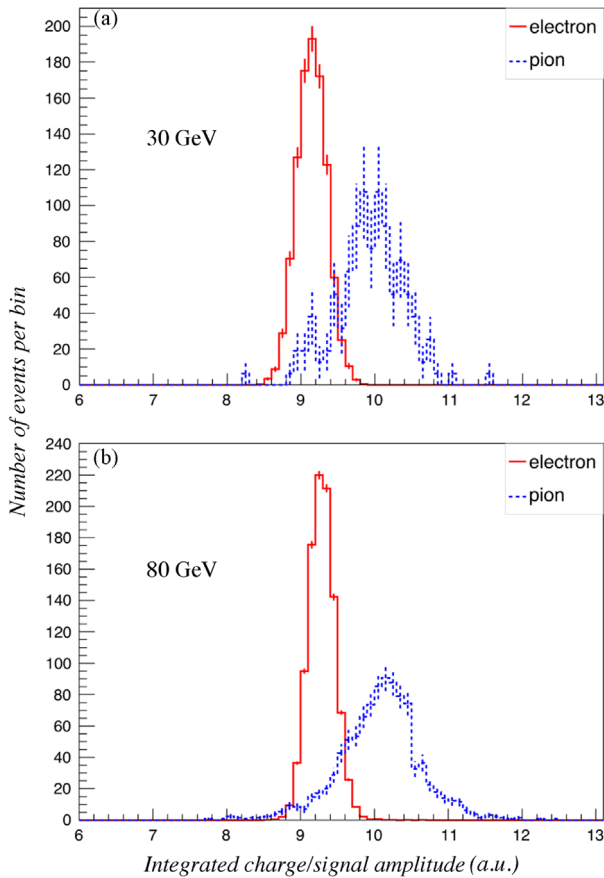


Fig. 11. Distribution of the ratio of the integrated charge and the amplitude of the signals produced by electrons and pions in one module of the RD52 fiber calorimeter. Data for 30 (a) and 80 GeV (b).

Table 4

The electron identification efficiency and the probability for mis-identifying a pion as an electron, for various choices of the parameter $(Q/A)_{\text{cut}}$, which defines a particle as an electron/pion when the ratio of the integrated charge and the pulse amplitude (Q/A) is smaller/larger than $(Q/A)_{\text{cut}}$. The statistical uncertainties in the electron identification efficiency are in all cases smaller than 0.1%.

$(Q/A)_{\text{cut}}$	30 GeV		80 GeV	
	e id (%)	π mis-id (%)	e id (%)	π mis-id (%)
9.3	90.1	12.0 ± 2.6	75.0	9.8 ± 0.6
9.4	96.1	17.1 ± 3.0	89.3	12.6 ± 0.7
9.5	98.6	20.3 ± 3.2	96.1	16.9 ± 0.8
9.6	99.7	26.6 ± 3.5	98.7	22.0 ± 0.9
9.7	99.9	35.4 ± 3.8	99.6	27.4 ± 1.0

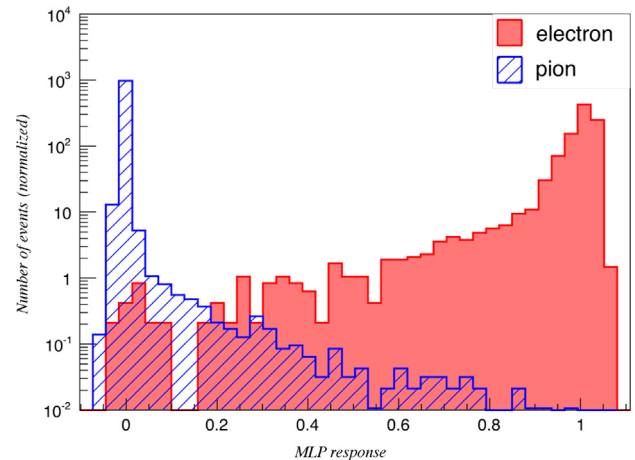


Fig. 12. Results from the multivariate analysis of the electron/pion separability at 60 GeV, which made simultaneous use of the lateral shower profile, the Cherenkov/scintillation signal ratio and the starting time of the PMT signals as the event characteristics that allowed distinguishing electrons from pions. The multi-layer perception (MLP) response indicates that 99.8% of all electrons could be identified with a combination of criteria that rules out 99.8% of all pions as electron candidates.

limit to the electron/pion separation achievable with the methods described in this paper. Even though the probability that electrons produce a mip signal in the PSD was not negligible ($\sim 10\%$), such contamination turned out to be not significant. This was concluded from analyzing the signal distributions from the leakage counters, and is a consequence of the fact that the secondary beams used for our studies consisted overwhelmingly of hadrons.

4. Discussion

We have shown that the longitudinally unsegmented RD52 fiber calorimeter can be used to identify electrons with a very high degree of accuracy. At 60 GeV, using the time structure of the signals, the lateral shower profile and a comparison of the Cherenkov and scintillation signals, more than 99% of the electrons entering the detector were correctly identified with criteria that rule out almost all hadronic particles as electron candidates. Longitudinal segmentation is thus most definitely not required for this purpose.

Other reasons often used for longitudinal segmentation include the possibility to optimize the energy resolution of the em section, while limiting at the same time the cost of the hadronic section. However, in future experiments at the next generation high-energy lepton–lepton colliders, excellent energy resolution is needed for *all* particles, not just electrons. Since sampling fluctuations are a major limiting factor both for electrons and hadrons in well designed dual-readout calorimeters, it stands to reason to use the same high sampling fraction and frequency throughout the calorimeter. This uniform structure is also a crucial factor for eliminating the intercalibration problems that plague *all* longitudinally segmented calorimeter systems [7,8].

On the other hand, elimination of longitudinal segmentation offers the possibility to make a finer lateral segmentation with the same number of electronic readout channels. This has many potential benefits. A fine lateral segmentation is crucial for recognizing closely spaced particles as separate entities. Because

of the extremely collimated nature of em showers,⁵ it is also a crucial tool for recognizing electrons in the vicinity of other showering particles. Moreover, as illustrated by Fig. 6, a fine lateral segmentation is important for the identification of electrons in general. Unlike the vast majority of other calorimeter structures used in practice, the RD52 fiber calorimeter offers almost limitless possibilities for lateral segmentation. If so desired, one could read out every individual fiber separately. Modern silicon PM technology certainly makes that a realistic possibility.

Acknowledgments

We thank CERN for making particle beams available to our experiments in the H8 beam. We gratefully acknowledge Eileen Hahn and Erik Ramberg of Fermilab who took care of the aluminization of the Cherenkov fibers used in one of the copper modules. This study was carried out with financial support of the United States Department of Energy, under contract DE-FG02-12ER41783, and by Italy's Istituto Nazionale di Fisica Nucleare and Ministero dell'Istruzione, dell'Università e della Ricerca.

References

- [1] N. Akchurin, et al., Nucl. Instrum. Methods Res. Sec. A 537 (2005) 537.
- [2] D.E. Groom, Nucl. Instrum. Methods Res. Sec. A 572 (2007) 633; D.E. Groom, Nucl. Instrum. Methods Res. Sec. A 697 (2013) 84.
- [3] R. Wigmans, New J. Phys. 10 (2008) 025003.
- [4] N. Akchurin et al., The electromagnetic performance of the RD52 fiber calorimeter, to be published in NIMA. <http://dx.doi.org/10.1016/j.nima.2013.09.033>.
- [5] R. Wigmans, Calorimetry, Energy Measurement in Particle Physics, International Series of Monographs on Physics, vol. 107, Oxford University Press, 2000.
- [6] D. Acosta, et al., Nucl. Instrum. Methods Res. Sec. A 302 (1991) 36.
- [7] M. Albrow, et al., Nucl. Instrum. Methods Res. Sec. A 487 (2002) 381.
- [8] R. Wigmans, On the calibration of segmented calorimeter systems, in: Proceedings of the XIIth International Conference on Calorimetry in High Energy Physics, Chicago 2006, AIP Conference Proceedings 867 (2006) 90.
- [9] M. Backes, et al., TMVA 4, Toolkit for Multivariate Data Analysis with ROOT, [arXiv:physics/0703039](http://arxiv.org/abs/physics/0703039).

⁵ Detailed measurements of the lateral profile of em showers in this calorimeter revealed a dominant central core with a diameter of only 3 mm [4].